Stem Cell Reports
Report

ISSCR

OPEN ACCESS

In Vivo Generation of Engraftable Murine Hematopoietic Stem Cells by *Gfi1b*, *c-Fos*, and *Gata2* Overexpression within Teratoma

Masao Tsukada,[1] Yasunori Ota,[2] Adam C. Wilkinson,[1,3] Hans J. Becker,[6] Motomi Osato,[4,5] Hiromitsu Nakauchi,[1,3,*] and Satoshi Yamazaki[1,6,*]

[1]Laboratory of Stem Cell Therapy, Center for Experimental Medicine, The Institute of Medical Science, The University of Tokyo, Tokyo 108-8639, Japan
[2]Department of Pathology, Research Hospital, The Institute of Medical Science, University of Tokyo, Tokyo 108-8639, Japan
[3]Institute for Stem Cell Biology and Regenerative Medicine, Stanford University School of Medicine, 265 Campus Drive, Stanford, CA 94305, USA
[4]Cancer Science Institute of Singapore, National University of Singapore, Singapore, Singapore
[5]International Research Center for Medical Sciences, Kumamoto University, Kumamoto, Japan
[6]Project Division of Advanced Regenerative Medicine, The Institute of Medical Science, The University of Tokyo, Tokyo 108-8639, Japan
*Correspondence: nakauchi@ims.u-tokyo.ac.jp (H.N.), y-sato4@ims.u-tokyo.ac.jp (S.Y.)
http://dx.doi.org/10.1016/j.stemcr.2017.08.010

SUMMARY

Generation of hematopoietic stem cells (HSCs) from pluripotent stem cells (PSCs) could potentially provide unlimited HSCs for clinical transplantation, a curative treatment for numerous blood diseases. However, to date, *bona fide* HSC generation has been largely unsuccessful *in vitro*. We have previously described proof of concept for *in vivo* HSC generation from PSCs via teratoma formation. However, our first-generation system was complex and the output low. Here, we further optimize this technology and demonstrate the following: (1) simplified HSC generation using transcription factor overexpression; (2) improved HSC output using *c-Kit*-deficient host mice, and (3) that teratomas can be transplanted and cryopreserved. We demonstrate that overexpression of *Gfi1b*, *c-Fos*, and *Gata2*, previously reported to transdifferentiate fibroblasts into hematopoietic progenitors *in vitro*, can induce long-term HSC formation *in vivo*. Our *in vivo* system provides a useful platform to investigate new strategies and re-evaluate existing strategies to generate HSCs and study HSC development.

INTRODUCTION

Pluripotent stem cells (PSCs) can differentiate into any bodily cell type. Somatic cells can also be reprogrammed to pluripotency by overexpression of "Yamanaka factors," generating inducible PSCs (iPSCs) (Takahashi and Yamanaka, 2006). Optimization of these technologies over the past 10 years has enabled the safe generation of patient-specific iPSCs for prospective clinical applications. Now the major hurdle in the translational application of iPSC technologies is developing strategies to differentiate PSCs into clinically relevant functional cell types.

Adult hematopoietic stem cells (HSCs) reside in the bone marrow (BM) and have the unique ability to reform the entire blood system (Eaves, 2015). HSC function is defined by a cell-intrinsic transcriptional program as well as cell-extrinsic signaling emanating from the BM microenvironment. Long-term HSC function provides the basis of BM transplantation, a curative therapy for a range of hematological disorders. Derivation of functional HSCs from PSCs has therefore been a long-sought goal of regenerative medicine (Wahlster and Daley, 2016). However, we are currently unable to generate truly functional HSCs from PSCs *in vitro*. This is likely due to our inability to fully recapitulate the complex and temporally dynamic *in vivo* microenvironmental signaling program that specifies HSCs during development (Medvinsky et al., 2011). In mice, transplantable HSCs emerge from hemogenic endothelial (HE) precursors, notably in the dorsal aorta (Zovein et al., 2008). Expression of the transcription factor (TF) *Runx1* can be used to track this process (North et al., 1999); live-cell imaging has captured hematopoietic stem/progenitor cell (HSPC) formation at sites of *Runx1*$^+$ HE cells (Bertrand et al., 2010; Boisset et al., 2010).

Certain attempts to generate HSCs thus far have used transgene overexpression to either direct the differentiation of PSCs, or alternatively, to transdifferentiate other somatic cell types. Several approaches have been reported to generate hematopoietic cells *in vitro* (Doulatov et al., 2013; Riddell et al., 2014; Sandler et al., 2014). In two very recent reports, conversion of mouse and human endothelial cells to engraftable HSCs was achieved by overexpression of several TFs (Sugimura et al., 2017; Lis et al., 2017).

In another study, Pereira et al. (2013) reported that overexpression of three TFs (*Gfi1b*, *c-Fos*, and *Gata2*) could transdifferentiate mouse fibroblasts into HE-like intermediates that could further mature into hematopoietic progenitor cells (HPCs). However, fully functional HSCs were not generated by this method.

As an alternative, we (and others) have previously demonstrated proof of concept for the *in vivo* generation of fully functional HSCs from PSCs via teratoma formation (Suzuki et al., 2013; Amabile et al., 2013). However, our first-generation *in vivo* differentiation system (Suzuki et al., 2013) had several limitations: (1) PSCs needed to be co-injected with OP9 stromal cells and hematopoietic

 © 2017 The Author(s).
This is an open access article under the CC BY-NC-ND license (http://creativecommons.org/licenses/by-nc-nd/4.0/).

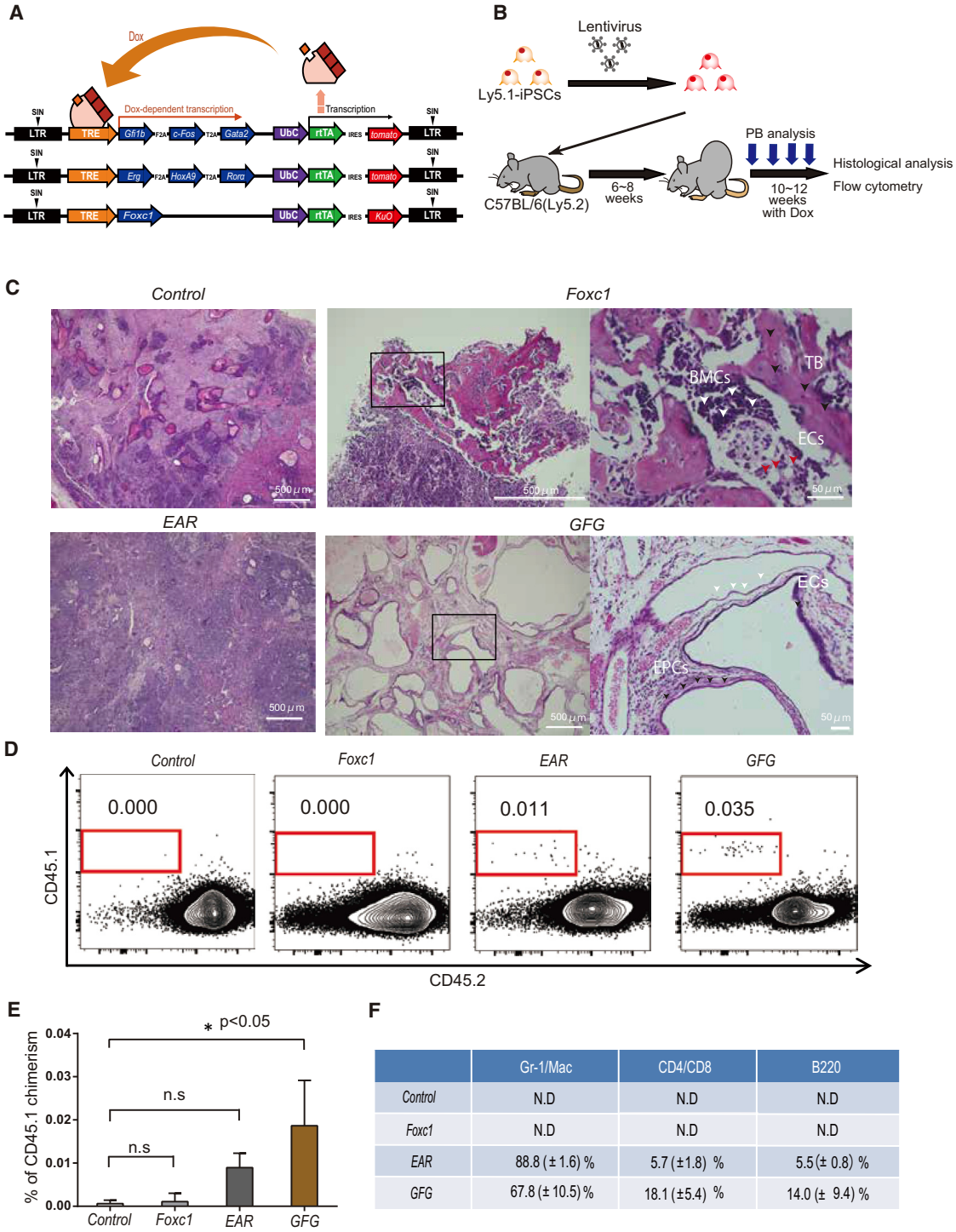

	Gr-1/Mac	CD4/CD8	B220
Control	N.D	N.D	N.D
Foxc1	N.D	N.D	N.D
EAR	88.8 (± 1.6) %	5.7 (±1.8) %	5.5 (± 0.8) %
GFG	67.8 (± 10.5) %	18.1 (±5.4) %	14.0 (± 9.4) %

Figure 1. Screening Transcription Factor Expression for Hematopoiesis within Teratomas

(A) Schematic diagram of the doxycycline (Dox)-inducible system for the expression of transcription factor (TF) combinations.

(B) Strategy to induce hematopoietic cells from lentivirally transduced iPSCs through teratoma formation. Dox was administrated for 4 weeks after teratoma size reached 2 cm in diameter, after which teratomas were collected for histological analysis.

(C) Representative H&E-stained teratoma sections, with morphological features labeled. Trabecular bone-like structure, TB (and black arrows); bone marrow cells, BMCs (and red arrows); endothelial cells, ECs (and white arrows); epithelial, EPCs (and black arrows).

(legend continued on next page)

cytokines (SCF and TPO) administered via micropump; (2) we could not identify the site of HSC emergence; and; (3) HSC formation was slow, taking 2–3 months. Here, we systemically overcome these limitations and provide an optimized *in vivo* HSC formation protocol. Furthermore, we demonstrate that *in vivo* overexpression of *Gfi1b*, *c-Fos*, and *Gata2* during teratoma formation is sufficient to generate functional long-term HSCs.

RESULTS

Gfi1b, *c-Fos*, and *Gata2* Overexpression Induces Hematopoietic Cell Formation in Teratomas

Teratomas contain tissues from all three germ layers, and we previously demonstrated that teratomas can generate HSCs (Suzuki et al., 2013). However, this required co-injection of OP9 stromal cells and continuous administration of cytokines (Suzuki et al., 2013). We hypothesized that induction of TFs related to HSCs and/or the HSC microenvironment could improve HSC generation in teratomas. To this end, we investigated three distinct TF combinations: (1) *Gfi1b*, *c-Fos*, and *Gata2* (*GFG*), which have been reported to generate HE-like cells and HPCs from fibroblasts (Pereira et al., 2013); (2) *Erg*, *HoxA9*, and *Rora* (*EAR*), which have been reported to generate HPCs during PSC embryoid body formation (Doulatov et al., 2013), and (3) *Foxc1*, reported to be highly expressed in *CXCL12*-abundant reticular (CAR) cells, an important component of the HSC BM niche (Omatsu et al., 2014).

To enable the identification of iPSC-derived HSCs, we first established iPSCs from a C57BL/6-Ly5.1 mouse to allow immunophenotypic discrimination from C57BL/6-Ly5.2 host mouse blood cells. Next, we cloned the above TFs into a doxycycline (Dox)-inducible (Tet-On) lentivirus expression vector (Figure 1A). Stable iPSC lines were generated and Dox-inducible transgene expression was confirmed using qPCR (Figure S1A). Next, we injected C57BL/6-Ly5.1 iPSCs (2×10^6) subcutaneously into host C57BL/6-Ly5.2 mice, and administered Dox for 4 weeks once teratomas reached >2 cm in diameter (6–8 weeks post-injection) to induce TF expression (Figure 1B). Importantly, this was undertaken without co-injection of stromal cells or cytokines.

After the 4-week Dox exposure, we analyzed the peripheral blood (PB) of engrafted mice by flow cytometry and the teratoma by histology (Figure 1B). We observed distinct differences between teratomas generated in the different experimental regimens (Figures 1C and 1D). For example, the *GFG* iPSC-derived teratomas contained a large number of endothelial and epithelial-like cells by H&E staining (Figure 1C). By contrast, *Foxc1*-derived teratomas formed bone cortices, cartilage, and BM-like cells (Figure 1C). While $CD45.1^+$ donor-derived blood cells were not detected in the host PB following injected with wild-type iPSCs or *Foxc1* iPSCs, both *EAR* iPSCs and *GFG* iPSCs reconstituted multi-lineage hematopoiesis 14–18 weeks post-injection (Figures 1D and 1E), with *GFG* iPSCs generating approximately 2-fold more hematopoietic cells (Figures 1E and 1F). These data demonstrate that *GFG* iPSC-derived teratomas differentiate into hematopoietic cells more efficiently compared with the other groups.

To evaluate the potential consequences of the *GFG* cassette on HSCs, we generated *GFG* transgenic mice from *GFG* embryonic stem cells. Leaky expression could not be detected (Figure S1B), and no difference in colony-forming ability was seen (Figure S1C). Reactivation of the reprogramming factors could also not be detected in iPSC-derived $CD45^+$ cells (Figure S1D).

Identification of Hemogenic Endothelium within GFG iPSC-Derived Teratomas

Given that *GFG* expression directly induces HE-like cells from mouse fibroblast *in vitro* (Pereira et al., 2013), we hypothesized that endothelial cells (ECs) within the *GFG* iPSC-derived teratomas (Figure 2A) might in fact resemble HE cells. By co-staining with Cytokeratin and CD31, we could identify $CD31^+$ endothelial-lined cystic structures, which were also $CD144/VE\text{-}cadherin^+$ (Figures S2A and S2B). We further confirmed the presence of *Runx1*-expressing ECs in *GFG* teratoma sections by immunostaining for Runx1 and CD31 (Figure 2B). Moreover, we could even identify hematopoietic cell clusters budding from these ECs (Figure 2B). $CD45^+$ hematopoietic cells could also be identified within the endothelial structures, suggesting teratoma vasculature was perfused with blood (Figure S2C).

Runx1 enhancer activity can be used to identify HE cells (Swiers et al., 2013). To study this in the teratoma, we established iPSCs from a *eR1-EGFP* transgenic reporter mouse (Ng et al., 2010). The activity of an enhancer for *Runx1* (eR1), formerly called *Runx1+24* or *+23,* is known to specifically mark HE cells within $CD31^+$ endothelium in the

(D) Representative flow cytometric plots of CD45.1 and CD45.2 expression in peripheral blood (PB) from teratoma-bearing Ly5.2 host mice at 14–16 weeks after Ly5.1 iPSC injection.

(E) Average percentage of $CD45.1^+$ PB cells in host mice. Data are the means ± SD from two independent experiments (n = 6). *p < 0.05.

(F) Average percentages of hematopoietic cell lineages within the $CD45.1^+$ population in (E). $Gr\text{-}1^+$, granulocytes; $Mac\text{-}1^+$, macrophages; $B220^+$, B cells; $CD4^+$, $CD4^+$ T cells; and $CD8^+$, $CD8^+$ T cells. Data are means ± SD from two independent experiments (n = 3).

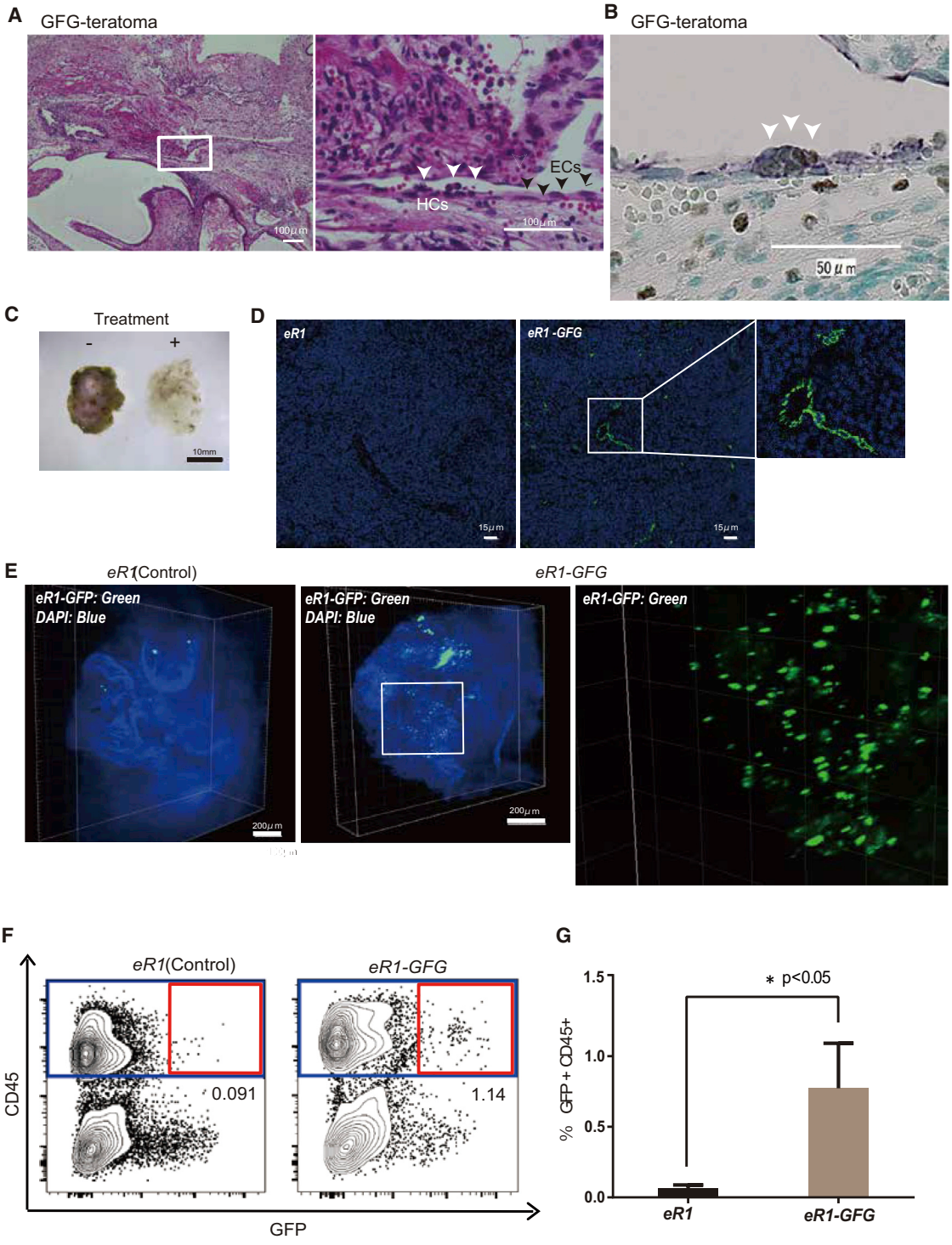

Figure 2. Identification of Hematopoietic-Generating Tissue in Teratomas

(A) Representative images from *GFG* teratoma sections stained with H&E. These tissues contain a large number of endothelial-like cells (ECs), annotated with black arrows. Hematopoietic cells (HCs) appearing to directly bud from ECs are annotated with white arrows.

(B) Representative images from *GFG* iPSC-derived teratoma sections stained with Runx1 and CD31. Runx1^{+} cells were detected by DAB (brown color) and CD31^{+} were detected by Bajoran purple (Purple color), with sites of double staining identified as putative sites of hematopoietic cell emergence, as marked by white arrows.

(legend continued on next page)

embryo as well as committed CD45$^+$ HSPCs (Nottingham et al., 2007). To comprehensively visualize all GFP$^+$ cells within the teratoma, we applied tissue clearing and 3D volumetric imaging or CUBIC (Susaki et al., 2014) (Figure 2C). Using this method, we were further able to identify GFP$^+$ endothelial structures within *GFG*-derived teratomas (Figures 2D and 2E). Notably, GFP$^+$ cells were much more frequent within the *GFG*-derived teratomas than the controls (Figure 2E).

We further confirmed that *eR1-EGFP*-iPSCs were giving rise to GFP$^+$CD45$^+$ HSPCs by flow cytometric analysis of the teratomas. We detected a distinct GFP$^+$CD45$^+$ cell population, which was nearly 10-fold higher in *GFG*-derived teratomas compared with the controls (average value: control, 0.06% ± 0.02%; *GFG*, 0.8% ± 0.3%) (Figures 2F and 2G). Therefore, *GFG* expression induces *eR1*-EGFP expression within teratomas and generates GFP$^+$CD45$^+$ hematopoietic cells, similar to that described *in vitro* (Pereira et al., 2013). However, the low frequency of teratoma-derived blood cells in this system precluded our further analysis of HSC formation and function. It is worth noting that GFG induction in iPSCs could not induce eR1-GFP expression, or surface markers associated with HE or hematopoietic cell commitment (Figure S2D), suggesting hematopoietic cell induction following GFG expression occurred within the context of teratoma development/differentiation.

Conditional c-Kit Deficiency Promotes Expansion of iPSC-Derived HSPCs *In Vivo*

Adult HSCs take up lifelong residence in the BM. To improve teratoma-derived hematopoietic cell frequencies, we hypothesized that HSC-deficient hosts would promote expansion of iPSC-derived HSCs. HSCs can engraft in *c-Kit*-deficient mice without irradiation (Cosgun et al., 2014). We therefore generated host mice with inducible, hematopoietic-specific *c-Kit* deletion by breeding C57BL/6-Ly5.2 *c-Kit$^{flox/flox}$ Mx1-Cre* transgenic mice where *c-Kit* deletion was achieved by poly(I:C) administration (Figure S3A). Importantly, white blood cell, hemoglobin, and platelet counts were lower in *c-Kit*-deficient mice (*c-Kit$^{\Delta/\Delta}$*) than in the controls (Figure S3B), and the BM was hypocellular (Figure S3C). We further confirmed long-term multi-lineage donor reconstitution in Ly5.2 *c-Kit$^{\Delta/\Delta}$* hosts without irradiation following transplantation of 1 × 10^7 Ly5.1 BM donor cells (Figures S3D and S3E).

Having validated a mouse model that was permissive to HSC engraftment, we next wanted to determine whether the *c-Kit$^{\Delta/\Delta}$* model could improve teratoma-derived HSC formation. We injected *GFG* iPSCs subcutaneously into *Mx1-Cre;c-Kit$^{flox/flox}$* host mice and administered poly(I:C) following teratoma formation (and Dox treatment) to deplete host HPSCs (Figure 3A). After 4–6 weeks, we observed a 10-fold increase in the frequency of iPSC-derived hematopoietic cells within the PB of the *c-Kit$^{\Delta/\Delta}$* hosts compared with control mice (control group, 0.02% ± 0.02%; *c-Kit $^{\Delta/\Delta}$*, 0.3% ± 0.2%) (Figure 3B). We also found similar increases in iPSC-derived cell frequencies within the BM (control group, 0.01% ± 0.001%; *c-Kit$^{\Delta/\Delta}$*, 0.2% ± 0.1%) (Figure 3C). Notably, poly(I:C) did not influence the generation of teratoma-derived PB cells in wild-type mice (Figure S4A).

To assess whether these hematopoietic cells contain engraftable HSCs, we transplanted 1 × 10^7 whole bone marrow cells (WBMCs) from teratoma-host mice into irradiated C57BL/6-Ly5.2 recipient mice (Figure 3A). We detected CD45.1$^+$ PB cells in multiple lineages over 16 weeks (Figure 3D). To functionally confirm long-term HSC capacity within the original CD45.1$^+$ cells, 1 × 10^7 WBMCs from the primary recipients were transplanted into irradiated secondary recipient mice. Multi-lineage CD45.1$^+$ PB cells could be detected long-term in these secondary recipients (and even in tertiary recipients), demonstrating long-term HSC activity (Figures 3D, S4B, and S4C). In addition, we detected immunophenotypic CD45.1$^+$C-KIT$^+$SCA-1$^+$Lineage$^-$ HPSCs in the BM of secondary recipients (Figure 3G). However, we noted that a 30% reduction in colony-forming units within the CD45.1$^+$ WBMC population compared with CD45.2$^+$ host BM cells, suggesting teratoma-derived BM cells are not identical to normally produced BM cells (Figures 3E, 3F, S4D, and S4E). However, these data demonstrate that *GFG* expression within teratomas generates functional HSCs that expand within *c-Kit*-deficient mice.

Transplantable Teratomas Provided Stable and Continuous Source of HSPCs

Finally, to improve on the time-consuming nature of these experiments, we investigated the following: (1) serial transplantation of freshly isolated teratomas and (2) use of cryopreservation of teratoma blocks. We performed transplantation of freshly isolated or cryopreserved teratoma blocks

(C) Representative images of teratoma tissue clearing in chemical cocktails and computational analysis (CUBIC); non-cleared on the left, cleared on the right.
(D) Localization of *eR1*$^+$ cells (green) and DAPI (blue) in 2D reconstructed image between *eR1*-derived and *eR1-GFG*-derived teratoma.
(E) Localization of *eR1*$^+$ cells (green) and DAPI (blue) in 3D reconstructed images between *eR1*-derived and *eR1-GFG*-derived teratoma.
(F) Representative flow cytometric plots for CD45 and GFP expression in the teratoma from *eR1*-EGFP iPSC-derived teratomas.
(G) Percentage GFP$^+$CD45$^+$ cells in teratomas, using gating displayed in (F) (n = 3). *p < 0.05.

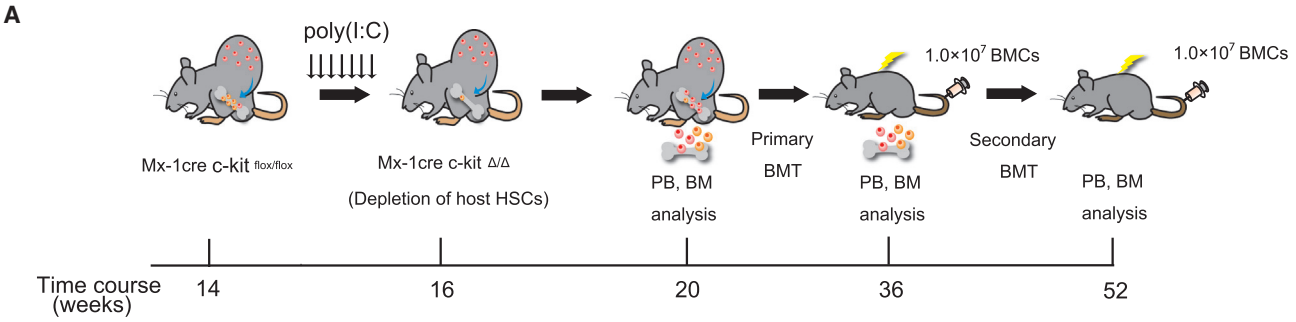

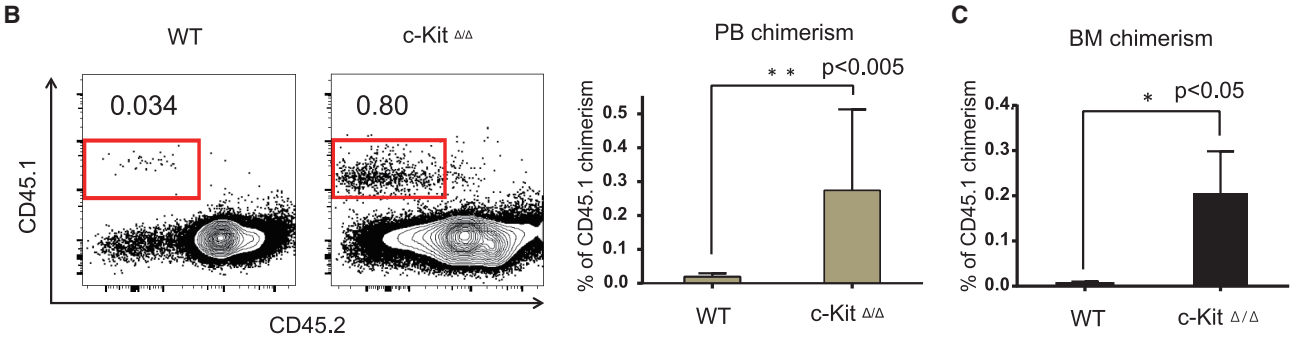

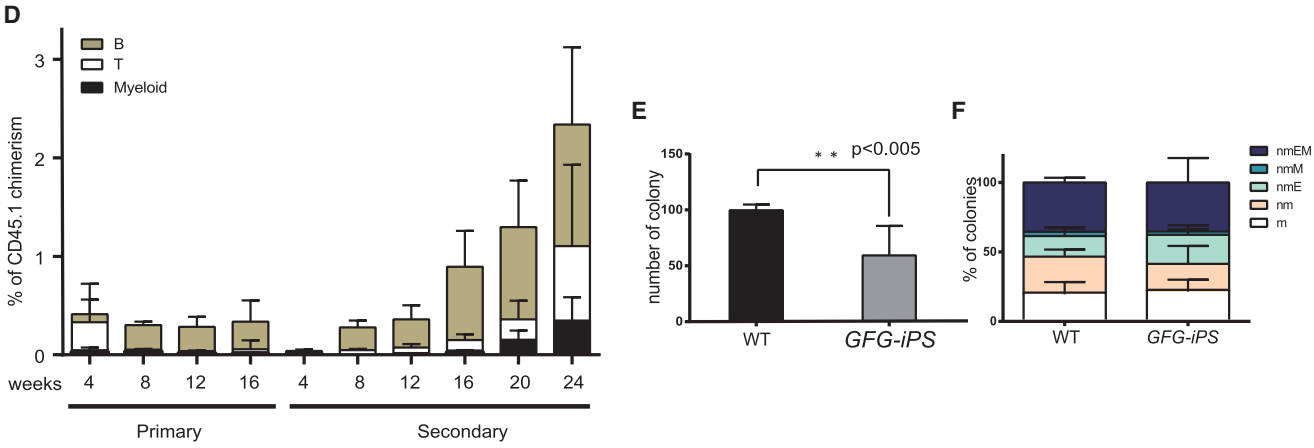

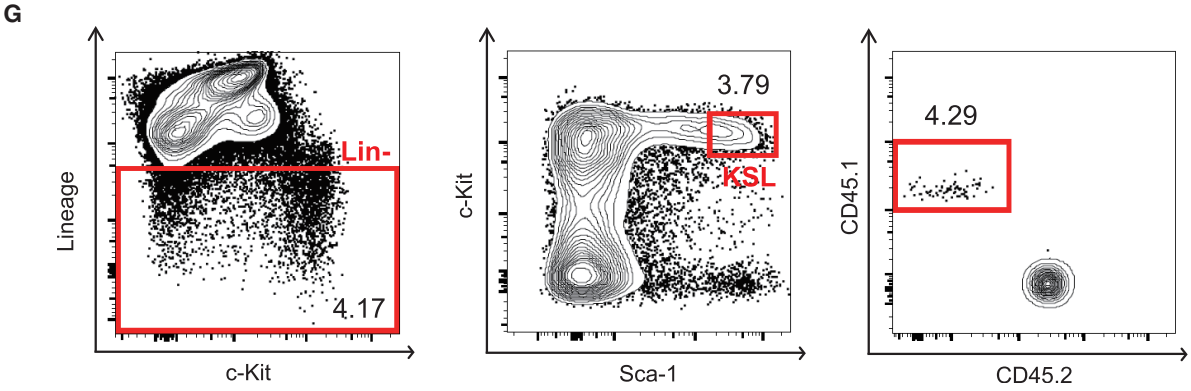

(legend on next page)

into host recipient mice (Figure 4A). In both cases, the transplanted teratomas survived and expanded (Figure 4B). Moreover, transplantable teratoma blocks generated hematopoietic cells that seeded the BM of *c-Kit*$^{\Delta/\Delta}$ host mice (Figure 4C). Using this transplantation approach, we are able to shorten hematopoietic cell generation time by 5 weeks, from 10 to 5 weeks (Figure 4D). The frequency of teratomas that generated CD45.1$^+$ blood cells was also higher in the transplanted hosts, compared with injection of iPSCs (Figure 4E). We also confirmed CD45.1$^+$ WBMCs from these hosts could transplant into recipients (Figure S4F). Combined, these data demonstrate that transplantable teratomas constitute stable and continuous sources of hematopoietic cells.

DISCUSSION

Here, we report an optimized system to generate HSC *in vivo* via teratoma formation for faster, higher-efficiency HSC production from iPSCs without co-injection of stromal cells or continuous provision of cytokines. While Pereira et al. (2013) were able to generate HPCs from fibroblasts *in vitro* by overexpressing *GFG*, transplantable HSCs could not be detected. Here, we have demonstrated that within an *in vivo* environment (iPSC-derived teratomas), *GFG* expression generated functional long-term HSCs. Our data therefore highlight the importance of *in vivo* evaluation of directed and transdifferentiation approaches. We envision *in vivo* HSC generation via teratoma formation as an important assay to assess new (and existing) approaches to generate engraftable HSCs. We also highlight the potential of our system to study mechanisms of HSC generation using an *eR1-EGFP* reporter system (Ng et al., 2010). In summary, we demonstrate that *GFG* overexpression *in vivo* within mouse teratomas can generate fully functional HSCs.

EXPERIMENTAL PROCEDURES

Mice

C57BL/6-Ly5.2 (Ly5.2) and C57BL/6-Ly5.1 (Ly5.1) mice were purchased from Japan SLC (Shizuoka, Japan) and Sankyo Lab Service (Tsukuba, Japan), respectively. For generation of *Mx1-Cre c-Kit*$^{flox/flox}$ mice, *c-Kit*$^{lox66\text{-}71/lox66\text{-}71}$ mice (Kimura et al., 2011) were crossed with *Mx1-Cre* mice transgenic mice (Kuhn et al., 1995). Mice received 250 μg of poly(I:C) intraperitoneally seven times every other day to induce Cre expression. Animal experiments were approved by the Animal Care and Use Committee, Institute of Medical Science, University of Tokyo.

Cell Culture

Mouse iPSCs were obtained by reprogramming tail-tip fibroblasts of C57BL/6-Ly5.1 mice with *Oct4*, *Sox2*, and *Klf4*, and then maintained as previously described (Nakagawa et al., 2008).

Lentivirus

Inducible lentivirus vectors were derived from the self-inactivating lentiviral vector CS-TRE-PRE-Ubc-tTA-I2G (Yamaguchi et al., 2012). Lentiviral production was performed as previously described (Shibuya et al., 2003).

Reverse Transcription PCR

Total RNA was extracted using TRIzol (Invitrogen) and reverse transcribed (High Capacity cDNA RT Kit; Applied Biosystems). qPCR was performed using the Universal Probe Library System (Roche Diagnostics; see Table S1). Samples were normalized to *Gadph* expression, using TaqMan probes (Applied Biosystems).

Teratoma Formation

Two million murine iPSCs were administered subcutaneously into C57BL/6(Ly5.2) or *Mx1-Cre* c-*Kit*$^{flox/flox}$ mice (6–10 weeks old) with Matrigel. We measured teratoma growth every month and analyzed the ratio of CD45.1$^+$ cells in PB every month. Where indicated, TF expression was induced after teratoma formation by Dox (2 μg/mL) administration via the water supply for 4 weeks.

Figure 3. *c-Kit* Deficiency Promotes Expansion of Hematopoietic Stem Cells from *GFG*-Derived iPSCs

(A) Strategy to induce HSCs from iPSCs using *c-Kit* deficient host mice. iPSCs were injected subcutaneously and Dox administered for 4 weeks to induce *GFG* expression (as in Figure 1B). Host mice were then administered polyI:C at weeks 14–16. At 20 weeks, WBMCs from teratoma-bearing mice were transplanted into irradiated mice, and PB/BM chimerism tracked. Secondary transplantations were performed at 16 weeks after the primary transplantation.

(B) Representative flow cytometric plots for CD45.1 and CD45.2 expression in the PB from teratoma-bearing C57BL/6 and *c-Kit*-deficient mice after 4–6 weeks poly(I:C) administration.

(C) Percentage CD45.1$^+$ chimerism in the PB (left) and BM (right). Data are the means ± SD from two independent experiments (n = 6). **p < 0.005, *p < 0.05.

(D) Percentage of (*GFG* iPSC-derived) CD45.1$^+$ PB chimerism of in primary and secondary recipient mice (n = 5).

(E and F) Colony potential of 2.0 × 10^4 host CD45.2$^+$ and *GFG*-derived CD45.1$^+$ BM cells of secondary recipients, after 11-day culture in Methocult. Total number of colonies displayed in (E) and colony type displayed in (F). Data are means ± SD from two independent experiments (n = 3). Colony cells were morphologically identified as neutrophils (n), macrophages (m), erythroblasts (E) and megakaryocytes (M). **p < 0.005.

(G) Representative flow cytometric plots and gating for the Kit$^+$Sca1$^+$Lineage$^-$ fraction within the BM of secondary recipient mice transplanted with *GFG* teratoma-derived blood cells 24 weeks post-transplantation. *Lin*$^-$, lineage negative cells; *KSL*, Lin$^-$Kit$^+$Sca1$^+$ cells.

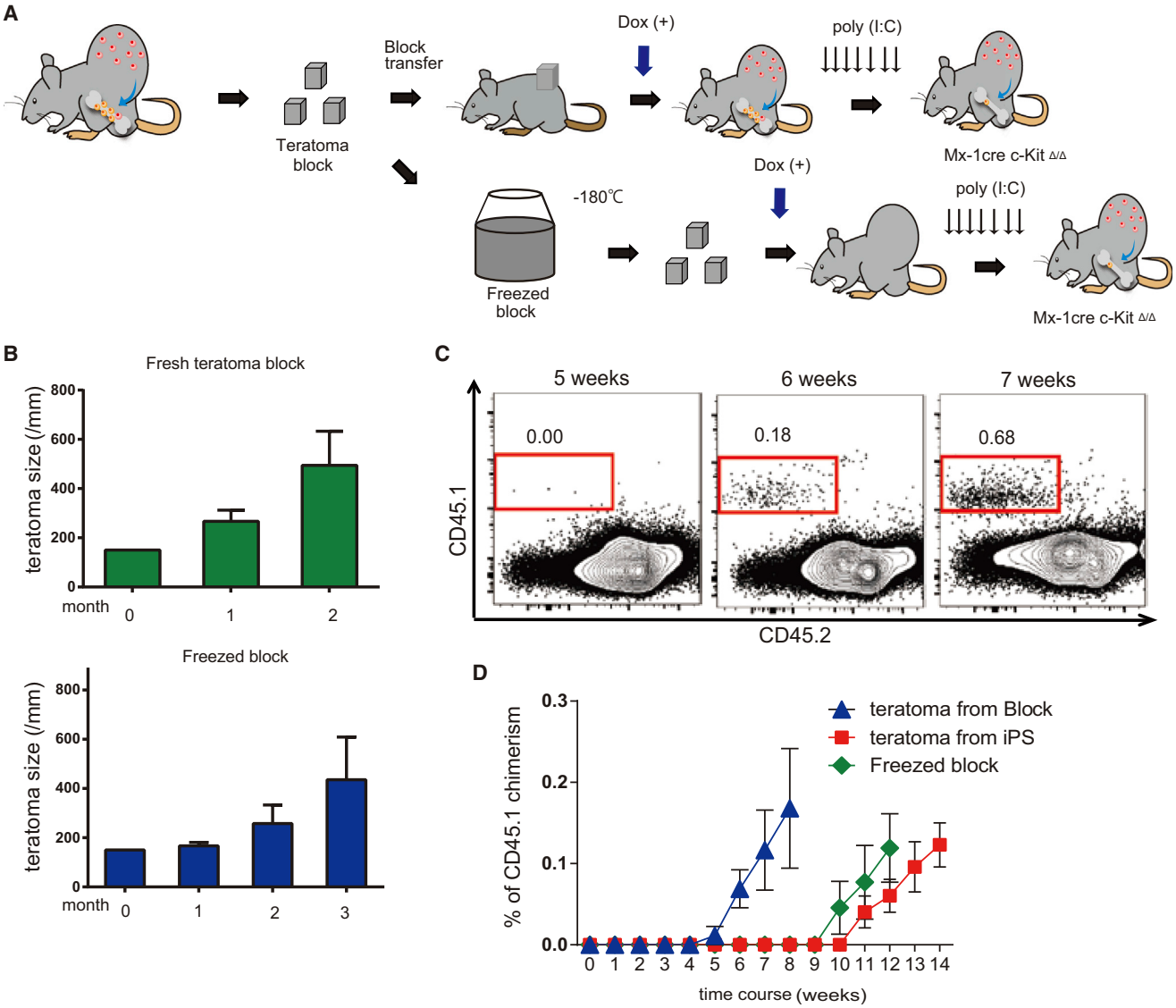

E

Origin	Frequency teratomas giving rise to CD45.1 cells
iPSCs	6/20 (30%)
Transplantable teratomas (generating blood cells)	16/25 (60%)
Transplantable teratomas (not generating blood cells)	2/25 (8.0%)
Cryptopreservation of teratomas	3/5 (60%)

Figure 4. Transplantation and Freeze Preservation of Teratoma Blocks

(A) Strategy transplant and freeze-preserved teratomas for hematopoietic cell formation. Teratomas (26–30 weeks old) were divided into (1.5 × 1.5 × 1.5 cm) blocks and were transplanted into *c-Kit*-deficient mice with 4 weeks of Dox administration (with or without initial freeze preservation), followed by poly(I:C) administration.

(B) Average diameter of the transplanted teratoma blocks after transplantation (n = 3).

(legend continued on next page)

After 4 weeks of Dox administration, mice received poly(I:C) intraperitoneally.

BM Transplantation Assay

BM cells (1×10^7) from teratoma-bearing mice were transplanted into lethally irradiated (9.5 Gy) wild-type C57BL/6-Ly5.2 recipient mice. BM cells (1×10^7) from the primary recipient mice were transplanted 16 weeks after primary BM transplantation into lethally irradiated secondary recipients.

Flow Cytometry

PB and BM were stained with anti-mouse antibodies as detailed in Table S2. Analysis was performed on a FACSCanto using Summit software (Beckman Coulter), and the results were analyzed with FlowJo.

Colony Assays

BM cells (20,000) were added to 1.1 mL of MethoCult GF M3434 (STEMCELL Technologies) and cultured at 37°C with 5% CO_2. Colonies were counted after 11 days, cytospun onto slide glasses, and subjected to Hemacolor staining (Merck) for morphological examination.

Histopathology/Immunohistochemistry

Histological findings were assessed by H&E-stained sections of paraffin-embedded teratoma tissue. For immunohistochemical analysis of teratomas, sections were stained with anti-Runx1 monoclonal Ab (Abcam92336) followed by anti-rabbit IgG-HRP. Antibody staining was detected by DAB staining followed by counterstaining with hematoxylin. After heating the microscope slides to 95°C for 5 min, sections were stained with anti-CD31 monoclonal Ab (SPRING BIOSCIENCE SP38) followed by anti-rabbit IgG-HRP. Antibody staining was detected by Bajoran Purple Chromogen Kit (Biocare Medical).

3D Teratoma Imaging

Teratoma clearing protocols were slightly modified from the original CUBIC protocol (Susaki et al., 2014). Teratomas were collected and fixed in 4% paraformaldehyde solution for 2 days. For nuclear staining, teratomas were immersed in DAPI/PBS solution at 37°C for 3 days with gentle shaking. Tissues were embedded in 4 mm diameter glass capillaries with 2% agarose for imaging. Images were acquired using a Zeiss Z1 Lightsheet microscope (Zeiss) and reconstituted into 3D images using Zen software (Zeiss).

Statistics

Calculations of statistically significant differences between samples using the Student's two-tailed t test were performed using Prism 4 software. Error bars displayed are the SD.

SUPPLEMENTAL INFORMATION

Supplemental Information includes four figures and two tables and can be found with this article online at http://dx.doi.org/10.1016/j.stemcr.2017.08.010.

AUTHOR CONTRIBUTIONS

M.T., Y.O., and S.Y. planned and performed the experiments and wrote the manuscript. M.O. helped perform experiments. A.C.W., H.J.B., and H.N. provided scientific discussion and technical support. S.Y., H.B., A.W., and H.N. directed the study and wrote the manuscript.

ACKNOWLEDGMENTS

We thank Y. Yamazaki, Y. Ishii, R. Ishida, K. Ito, S. Rafii, M. Otsu, and R. Yamamoto for support and advice. This work was supported by grants from the Japan Society for the Promotion of Science (JSPS) (grant no. 50625580), the Ministry of Education, Culture, Sport, Science, and Technology (Japan), the California Institute of Regenerative Medicine (grant no. LA1-06917), the Siebel Foundation, and the Ludwig Foundation. A.C.W. is a Bloodwise Visiting Fellow.

Received: December 29, 2016
Revised: August 18, 2017
Accepted: August 18, 2017
Published: September 21, 2017

REFERENCES

Amabile, G., Welner, R.S., Nombela-Arrieta, C., D'Alise, A.M., Di Ruscio, A., Ebralidze, A.K., Kraytsberg, Y., Ye, M., Kocher, O., Neuberg, D.S., et al. (2013). In vivo generation of transplantable human hematopoietic cells from induced pluripotent stem cells. Blood *121*, 1255–1264.

Bertrand, J.Y., Chi, N.C., Santoso, B., Teng, S., Stainier, D.Y.R., and Traver, D. (2010). Haematopoietic stem cells derive directly from aortic endothelium during development. Nature *464*, 108–111.

Boisset, J.-C., van Cappellen, W., Andrieu-Soler, C., Galjart, N., Dzierzak, E., and Robin, C. (2010). In vivo imaging of haematopoietic cells emerging from the mouse aortic endothelium. Nature *464*, 116–120.

Cosgun, K.N., Rahmig, S., Mende, N., Reinke, S., Hauber, I., Schäfer, C., Petzold, A., Weisbach, H., Heidkamp, G., Purbojo, A., et al. (2014). Kit regulates HSC engraftment across the human-mouse species barrier. Cell Stem Cell *15*, 227–238.

Doulatov, S., Vo, L.T., Chou, S.S., Kim, P.G., Arora, N., Li, H., Hadland, B.K., Bernstein, I.D., Collins, J.J., Zon, L.I., et al. (2013). Induction of multipotential hematopoietic progenitors from human

(C) Representative flow cytometric plots for CD45.1 and CD45.2 from the PB of host mice 5–7 weeks after transplantation with *GFG* teratoma blocks (n = 5).
(D) Average percentage CD45.1$^+$ PB cells in host mice following transplantation with teratoma blocks, frozen blocks, or iPSCs. Data are the means ± SD from two independent experiments (n = 6 iPSCs, n = 16 teratoma blocks, n = 3 frozen blocks).
(E) Frequency of teratomas giving rise to CD45.1 PB cells from transplanted iPSCs and teratoma blocks.

pluripotent stem cells via respecification of lineage-restricted precursors. Cell Stem Cell *13*, 459–470.

Eaves, C.J. (2015). Hematopoietic stem cells: concepts, definitions, and the new reality. Blood *125*, 2605–2613.

Kimura, Y., Ding, B., Imai, N., Nolan, D.J., Butler, J.M., and Rafii, S. (2011). c-Kit-mediated functional positioning of stem cells to their niches is essential for maintenance and regeneration of adult hematopoiesis. PLoS One *6*, e26918.

Kuhn, R., Schwenk, F., Aguet, M., and Rajewsky, K. (1995). Inducible gene targeting in mice. Science *269*, 1427–1429.

Lis, R., Karrasch, C.C., Poulos, M.G., Kunar, B., Redmond, D., Duran, J.G.B., Badwe, C.R., Schachterle, W., Ginsberg, M., Xiang, J., et al. (2017). Conversion of adult endothelium to immunocompetent haematopoietic stem cells. Nature *545*, 439–445.

Medvinsky, A., Rybtsov, S., and Taoudi, S. (2011). Embryonic origin of the adult hematopoietic system: advances and questions. Development *138*, 1017–1031.

Nakagawa, M., Koyanagi, M., Tanabe, K., Takahashi, K., Ichisaka, T., Aoi, T., Okita, K., Mochiduki, Y., Takizawa, N., and Yamanaka, S. (2008). Generation of induced pluripotent stem cells without Myc from mouse and human fibroblasts. Nat. Biotechnol. *26*, 101–106.

Ng, C.E.L., Yokomizo, T., Yamashita, N., Cirovic, B., Jin, H., Wen, Z., Ito, Y., and Osato, M. (2010). A Runx1 intronic enhancer marks hemogenic endothelial cells and hematopoietic stem cells. Stem Cells *28*, 1869–1881.

North, T., Gu, T.L., Stacy, T., Wang, Q., Howard, L., Binder, M., Marín-Padilla, M., and Speck, N.A. (1999). Cbfa2 is required for the formation of intra-aortic hematopoietic clusters. Development *126*, 2563–2575.

Nottingham, W.T., Jarratt, A., Burgess, M., Speck, C.L., Cheng, J.-F., Prabhakar, S., Rubin, E.M., Li, P.-S., Sloane-Stanley, J., Kong-A-San, J., et al. (2007). Runx1-mediated hematopoietic stem-cell emergence is controlled by a Gata/Ets/SCL-regulated enhancer. Blood *110*, 4188–4197.

Omatsu, Y., Seike, M., Sugiyama, T., Kume, T., and Nagasawa, T. (2014). Foxc1 is a critical regulator of haematopoietic stem/progenitor cell niche formation. Nature *508*, 536–540.

Pereira, C.F., Chang, B., Qiu, J., Niu, X., Papatsenko, D., Hendry, C.E., Clark, N.R., Nomura-Kitabayashi, A., Kovacic, J.C., Ma'Ayan, A., et al. (2013). Induction of a hemogenic program in mouse fibroblasts. Cell Stem Cell *13*, 205–218.

Riddell, J., Gazit, R., Garrison, B.S., Guo, G., Saadatpour, A., Mandal, P.K., Ebina, W., Volchkov, P., Yuan, G.C., Orkin, S.H., et al. (2014). Reprogramming committed murine blood cells to induced hematopoietic stem cells with defined factors. Cell *157*, 549–564.

Sandler, V.M., Lis, R., Liu, Y., Kedem, A., James, D., Elemento, O., Butler, J.M., Scandura, J.M., and Rafii, S. (2014). Reprogramming human endothelial cells to haematopoietic cells requires vascular induction. Nature *511*, 312–318.

Shibuya, K., Shirakawa, J., Kameyama, T., Honda, S.-I., Tahara-Hanaoka, S., Miyamoto, A., Onodera, M., Sumida, T., Nakauchi, H., Miyoshi, H., et al. (2003). CD226 (DNAM-1) is involved in lymphocyte function-associated antigen 1 costimulatory signal for naive T cell differentiation and proliferation. J. Exp. Med. *198*, 1829–1839.

Sugimura, R., Jha, D.K., Han, A., Soria-Valles, C., da Rocha, E.L., Lu, Y.-F., Goettel, J.A., Serrao, E., Rowe, R.G., Malleshaiah, M., et al. (2017). Haematopoietic stem and progenitor cells from human pluripotent stem cells. Nature *545*, 432–438.

Susaki, E.A., Tainaka, K., Perrin, D., Kishino, F., and Tawara, T. (2014). Resource whole-brain imaging with single-cell resolution using chemical cocktails and computational analysis. Cell *157*, 726–739.

Suzuki, N., Yamazaki, S., Yamaguchi, T., Okabe, M., Masaki, H., Takaki, S., Otsu, M., and Nakauchi, H. (2013). Generation of engraftable hematopoietic stem cells from induced pluripotent stem cells by way of teratoma formation. Mol. Ther. *21*, 1424–1431.

Swiers, G., Baumann, C., O'Rourke, J., Giannoulatou, E., Taylor, S., Joshi, A., Moignard, V., Pina, C., Bee, T., Kokkaliaris, K.D., et al. (2013). Early dynamic fate changes in haemogenic endothelium characterized at the single-cell level. Nat. Commun. *4*, 2924.

Takahashi, K., and Yamanaka, S. (2006). Induction of pluripotent stem cells from mouse embryonic and adult fibroblast cultures by defined factors. Cell *126*, 663–676.

Wahlster, L., and Daley, G.Q. (2016). Progress towards generation of human haematopoietic stem cells. Nat. Cell Biol. *18*, 1111–1117.

Yamaguchi, T., Hamanaka, S., Kamiya, A., Okabe, M., Kawarai, M., Wakiyama, Y., Umino, A., Hayama, T., Sato, H., Lee, Y.S., et al. (2012). Development of an all-in-one inducible lentiviral vector for gene specific analysis of reprogramming. PLoS One *7*, e41007.

Zovein, A.C., Hofmann, J.J., Lynch, M., French, W.J., Turlo, K.A., Yang, Y., Becker, M.S., Zanetta, L., Dejana, E., Gasson, J.C., et al. (2008). Fate tracing reveals the endothelial origin of hematopoietic stem cells. Cell Stem Cell *3*, 625–636.

Stem Cell Reports, Volume *9*

Supplemental Information

In Vivo Generation of Engraftable Murine Hematopoietic Stem Cells by *Gfi1b, c-Fos*, and *Gata2* Overexpression within Teratoma

Masao Tsukada, Yasunori Ota, Adam C. Wilkinson, Hans J. Becker, Motomi Osato, Hiromitsu Nakauchi, and Satoshi Yamazaki

Supplementary Information

Supplementary Tables

Supplementary Table 1: qPCR primer and probe list

Gene	Forward (5' to 3')	Reverse (3' to 5')	Roche universal probe no.
Gfi1b	gcacagagtctcccttggac	atgaggggtggagaacacc	80
cFos	gggacagcctttcctactaccc	agatctgcgcaaaagtcctg	67
Gata2	gcttcacccctaagcagaga	atctcgtcgccagagagg	76
Erg	catgagtctccggaaagcag	tgaagcacaacaccttctataaactt	53
HoxA9	tccctgactgactatgcttgtg	gttggcagccgggttatt	25
Rora	cctactgttccttcaccaacg	tgttctgggcaaggtgttc	60
FoxC1	gctttcctgctcattcgtctt	aaatatcttacaggtgagaggcaag	34
Oct3/4	aatgccgtgaagttggagaa	ccttctgcagggctttcat	95
Sox2	acagctacgcgcacatga	ggtagcccagctgctcct	19
Klf4	cgggaagggagaagacact	gagttcctcacgccaacg	62

Supplementary Table 2: Antibody staining list

Peripheral blood antibody staining	Bone marrow antibody staining
CD45.1-PE-Cy7 (#560578 BD Biosciences)	Biotinylated lineage cocktail (#130-092-613（Miltenyibiotec）
CD45.2-FITC (#109806 BioLegend)	CD45.1-PB (#553776 BD Biosciences)
CD4-APC (#100515 BioLegend)	CD45.2-FITC (#109805 BioLegend)
CD8-APC (#17-0088-42 eBioscience),	Sca1-PE-Cy7 (#558162 PharMingen)
B220-APC-Cy7 (#25-0452-82 eBioscience)	cKit-APC (#553356 PharMingen)
Gr1-Pacific Blue (PB) (#108430 BioLegend)	Streptavidin-APC-Cy7 (#554063 PharMingen)
Mac-1-PB (#101224 BioLegend)	

Supplementary Figures

Supplementary Figure and Legends:

Figure S1

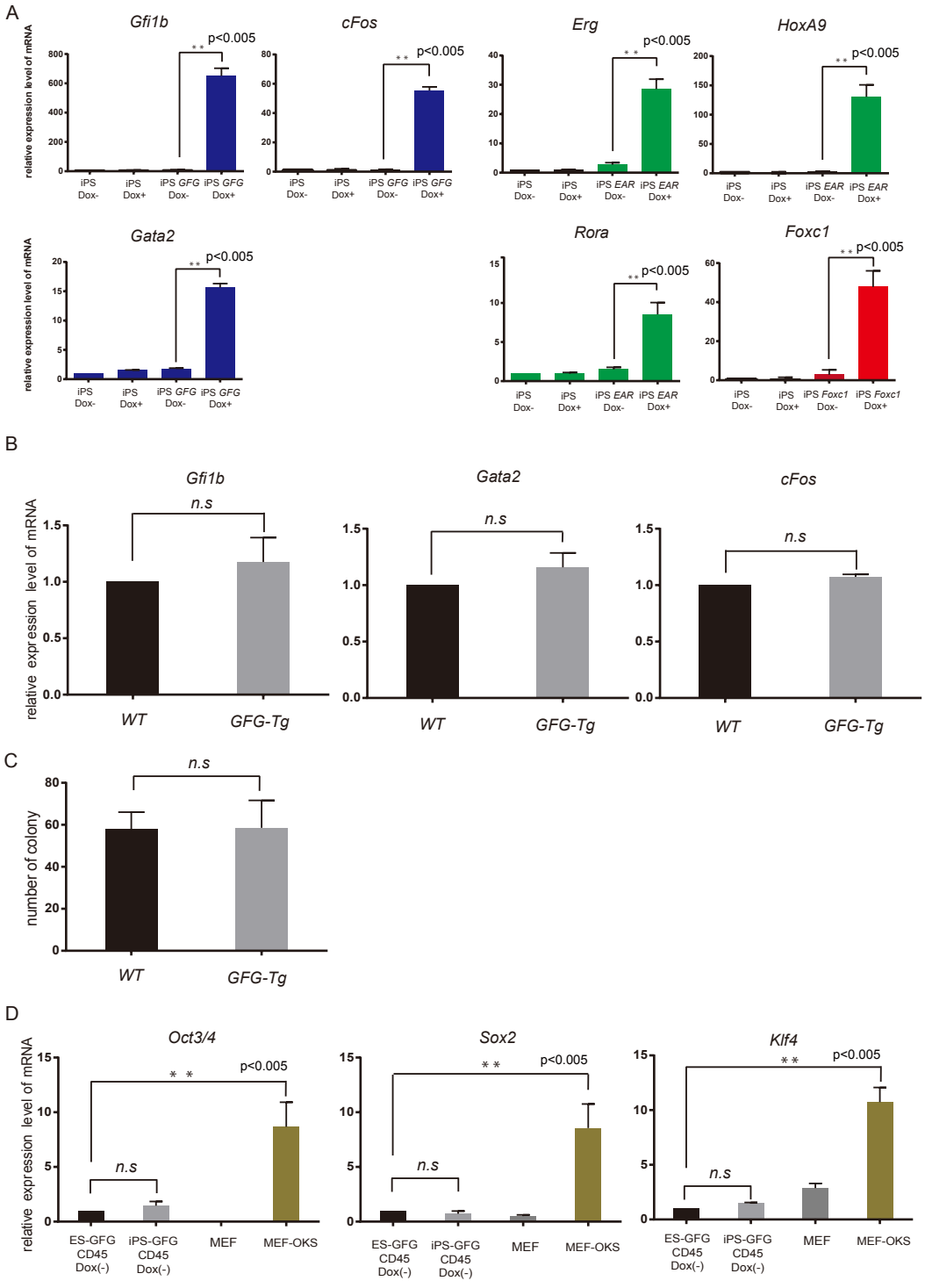

Figure S1: Related to Figure 1; establishment of inducible iPSCs from Ly5.1 mice

(A) Average relative transgene expression in iPSCs following a four-day induction by addition of Dox. Data are the mean ± SD from two independent experiments (n = 3). **P* < 0.005.

(B) Expression analysis of *Gfi1b*, *Gata2* and *cFos* in WBMCs of GFG transgenic mice (GFG-Tg) without Dox. Data are the mean ± SD from two independent experiments (n = 3). n.s : not significant.

(C) Colony formation from WBMCs isolated from wild type mice and GFG-Tg mice without Dox. Data are the mean ± SD from two independent experiments (n = 3). n.s : not significant.

(D) Analysis of reactivation of *Oct*, *Sox2* and *Klf4* genes using pluripotent stem cells derived $CD45^{+}$ cells by in vitro embryoid body differentiation and MEF. MEF-OKS group is positive control. Data are the mean ± SD from two independent experiments (n = 5). n.s : not significant.

Figure S2

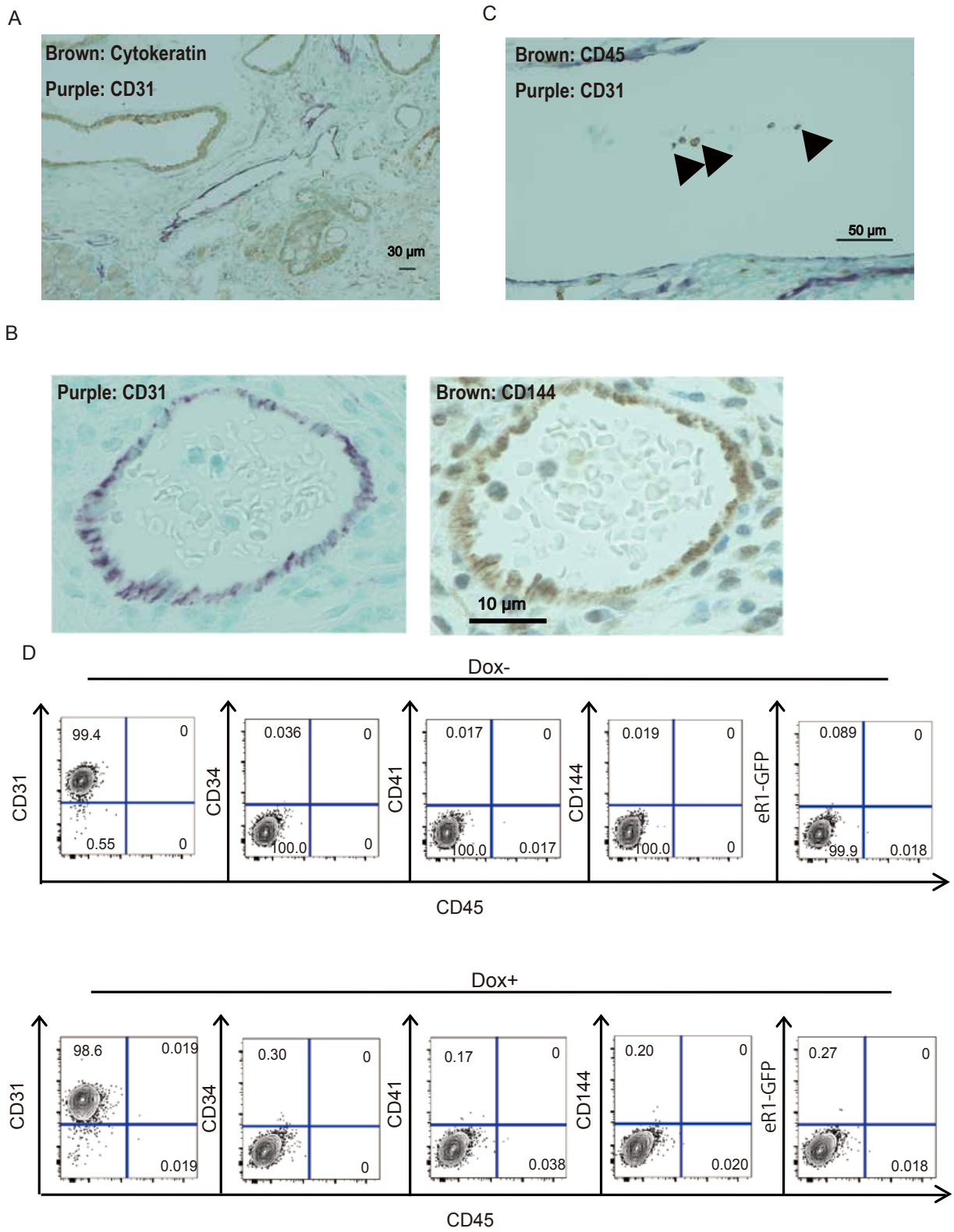

Figure S2: Related to Figure 2; analysis of hematopoietic-generating tissue in teratomas
(A) Representative image of a section of an GFG-teratoma immunostained for vascular

endothelial cells ($CD31^+$ cells; purple) and epithelial cells (Cytokeratin; brown).
(B) Serial sections of an GFG-teratoma immunostained for vascular endothelial cell markers CD31 (purple) and CD144 (brown).
(C) Representative image of a section of an GFG-teratoma immunostained for vascular endothelial cells ($CD31^+$ cells; purple) and hematopoietic cells ($CD45^+$ cells; brown).
(D) Representative flow cytometric plots displaying hematopoietic lineage marker expression on GFG-transduced eR1-iPSCs after four days cultured with or without dox.

Figure S3

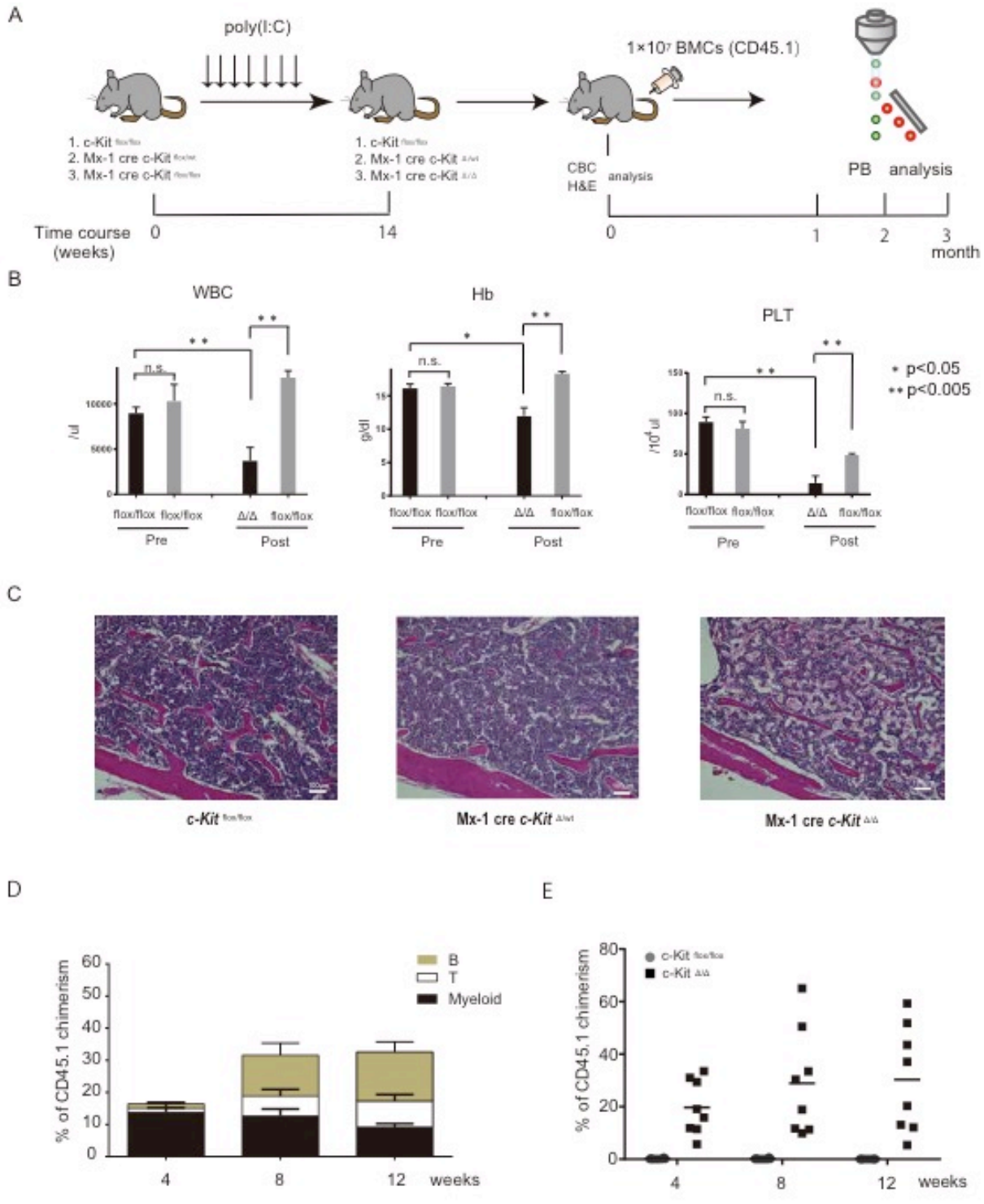

Figure S3: Related to Figure 3; analysis of hematopoiesis in *c-Kit* deficient mice

(A) Schematic of the strategy to validate HSPC-deficient host mice. CBC, histological analysis and hematopoietic reconstitution assay were undertaken following poly(I:C) administration.

(B) CBC was tested in peripheral blood (PB) from two groups of mice: poly(I:C)-treated (*c-Kit*-

deficient mice; black bars) and PBS-treated (control mice; grey bars). CBCs were tested both pre- and post-treatment. WBC: white blood cell, Hb: hemoglobin, PLT: platelet. Data are the mean ± SD from two independent experiments (n = 6 per group). $**P < 0.005$, $*P < 0.05$, n.s : not significant.

(C) *c-Kit* deficiency leads to impaired hematopoiesis. Femurs section from the control and *c-Kit*-deficient mice stained with hematoxylin-eosin.

(D, E) Donor-derived PB cell ratio was measured 12 weeks after transplantation into poly (I:C administrated recipients together with 1×10^7 bone marrow (BM) cells (CD45.1). (n=8)

Figure S4

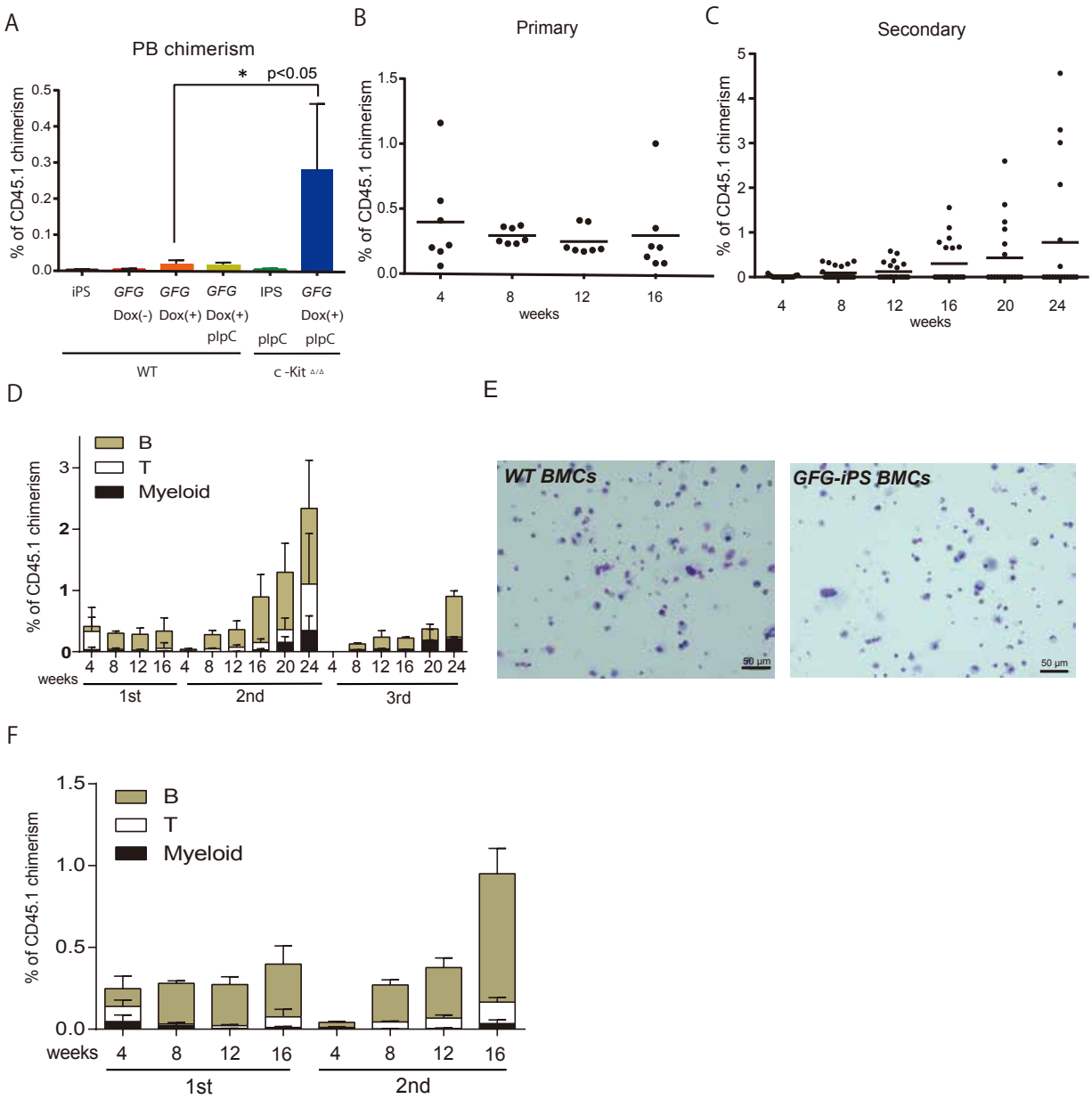

Figure S4: Related to Figure 3 and 4; *c-Kit* deficiency affords long-term HSC formation

from *GFG*-teratomas

(A) Percentage of CD45.1$^+$ PB chimerism in teratoma-bearing C57BL/6 mice and *c-Kit*-deficient mice at 14-16 weeks after iPSCs injection. Data are the mean ± SD (n = 8 *$P < 0.05$).

(B,C) Percentage of CD45.1$^+$ PB chimerisms in primary (B) and secondary (C) recipients of the bone marrow transplantation assay described in Figure 3D. Data are the mean ± SD from two independent experiments (n = 8 primary n=21 secondary)

(D) Percentage of CD45.1$^+$ PB chimerisms in primary, secondary, and tertiary recipients of BM from teratoma-bearing host mice. Data are the mean ± SD from two independent experiments. (n=5)

(E) Cytospin images of CFUs from the colony-forming assay with *GFG*-iPSC derived BMCs from recipient mice after secondary transplantation (n=5).

(F) Percentage CD45.1$^+$ PB chimerism analysis of teratoma block-derived BM cells after transplanting into primary and secondary recipient mice. Data are the mean ± SD from two independent experiments (n=5).

(E) Frequency teratomas giving rise to CD45.1$^+$ PB cells, from various origins (n=5).